Mechanics of balsa (*Ochroma pyramidale*) wood

Marc Borrega, Lorna J. Gibson

Department of Materials Science and Engineering, Massachusetts Institute of Technology, 77 Massachusetts Avenue, 02139 Cambridge MA, USA

Abstract

Balsa wood is one of the preferred core materials in structural sandwich panels, in applications ranging from wind turbine blades to boats and aircraft. Here, we investigate the mechanical behavior of balsa as a function of density, which varies from roughly 60 to 380 kg/m^3. In axial compression, bending, and torsion, the elastic modulus and strength increase linearly with density while in radial compression, the modulus and strength vary nonlinearly. Models relating the mechanical properties to the cellular structure and to the density, based on deformation and failure mechanisms, are described. Finally, wood cell-wall properties are determined by extrapolating the mechanical data for balsa, and are compared with the reduced modulus and hardness of the cell wall measured by nanoindentation.

Introduction

Balsa (*Ochroma pyramidale*), a tropical hardwood native to the Americas, is one of the fastest growing wood species, reaching about 20 m in height and up to 75 cm in diameter in 5-8 years (Fletcher 1951). Most balsa wood used commercially is harvested from plantations, particularly from Ecuador. Because of its fast growth, the wood density is very low, making balsa the lightest commercial timber available. Density values for balsa typically range between 100 and 250 kg/m^3, although they can vary as much as from 60 to 380 kg/m^3. The low density is extremely valuable in applications that require lightweight materials with good mechanical performance. Balsa wood is one of the preferred core materials in structural sandwich panels for wind turbine blades, sporting equipment, boats and aircraft.

The large density variations in balsa derive predominantly from the fibers (Borrega et al. 2014), long prismatic cells that act as the main load-bearing elements in wood. Consequently, the mechanical performance of balsa is strongly dependent on its density. The axial compressive Young's modulus and strength increase linearly with density, reaching values up to 6 GPa for modulus and 40 MPa for strength at the highest densities (Da Silva and Kyriakides 2007). The failure mode in compression transitions from plastic buckling of fibers to kink band formation as the density increases (Vural and Ravichandran 2003; Da Silva and Kyriakides 2007). Kink band formation in high density balsa is facilitated by local misalignment of fibers due to the presence of rays (parenchyma cells), which leads to the development of shear stresses during compression. The shear modulus and strength in balsa vary linearly with density, reaching values up to 350 MPa for modulus and 5 MPa for strength (Da Silva and Kyriakides 2007). In the transverse direction, compressive modulus and strength vary roughly with the cube and square of density, respectively, due to bending of the fiber cell walls (Easterling et al. 1982). Transverse compressive modulus and strength values are about an order of magnitude lower than those in the axial direction. The transverse compressive modulus and strength are higher in the radial than in the tangential direction because the rays act as reinforcement.

The mechanical properties of balsa have been modeled, particularly in compression, by considering the wood structure to resemble a honeycomb (Easterling et al. 1982; Gibson and Ashby 1997; Vural and Ravichandran 2003; Da Silva and Kyriakides 2007). Although this assumption is a simplification of the heterogeneous cellular structure in wood, the models have proven to be useful in describing its mechanical properties over a wide range of densities. As a cellular solid, the mechanical behavior of balsa (and other woods) depends on the properties of the material from which the cell walls are made. The dry density of the cell wall material is about 1469 kg/m^3 for all woods (Kellogg and Wangaard 1969), and thus the relative density of balsa, that is, the density of balsa divided by that of the cell wall, is generally lower than 0.25. The mechanical properties of the cell walls of wood have been determined by extrapolating mechanical data for several woods of widely different densities; extrapolated values for axial cell-wall Young's modulus and strength are about 35-40 GPa and 120 MPa, respectively (Cave 1969; Gibson and Ashby 1997).

The axial cell-wall Young's modulus has also been determined by a number of direct methods, including tensile tests of isolated fibers and bending of a fiber cell wall. Measured values for modulus are generally lower than those obtained by extrapolation. A mean axial cell-wall modulus of about 20 GPa has been obtained by tensile tests on mechanically and chemically isolated spruce fibers, but this elastic modulus was probably affected by mechanical damage and degradation of structural components during the isolation procedures (Burgert et al. 2005). Alternatively, an axial cell-wall modulus of about 28 GPa has been obtained by Orso et al. (2006) by bending of cantilever beams, which were produced with a focused ion beam (FIB) from the cell wall of spruce fibers. The axial compressive strength of the secondary cell wall in spruce, Keranji and Loblolly pine fibers, measured on micropillars machined by FIB, was 120-160 MPa (Zhang et al. 2010; Adusumalli et al. 2010). Typical values for the reduced modulus of the cell-wall measured by nanoindentation range from 16 to 24 GPa (Gindl et al. 2004; Wu et al. 2009). However, this technique tends to underestimate the cell-wall modulus because it reflects a combination of both axial and transverse properties, arising from the anisotropy of the wood cell wall.

The relatively high mechanical properties of balsa, for its density, make it attractive for cores in sandwich panels. To date, there are no engineered materials suitable for sandwich panel cores with a similar combination of mechanical properties and low density. With a view towards guiding the design of engineering materials inspired by balsa, we recently conducted a detailed characterization of its structure and composition (see Borrega et al. 2014). In this paper, we investigate its mechanical behavior over a wide range of densities and analyze the failure mechanisms under different loading conditions, relevant to the use of balsa wood in structural sandwich panels. The reduced modulus and hardness of the cell wall are also measured by nanoindentation. The mechanical properties are then modeled using existing models for cellular materials, microstructural data for balsa, and cell-wall properties determined by extrapolating the results from mechanical testing of macroscopic balsa specimens.

Structure and composition of balsa wood

The cellular structure in balsa wood consists of fibers (66-76%), rays (20-25%) and vessels (3-9%) (Borrega et al. 2014). The vessels are long tubular structures that run axially along the trunk of the tree and transport fluids from the roots to the crown. Their building blocks are known as vessel elements. The rays are brick-like parenchyma cells that run radially from the central pith to the outer part of the trunk. Their main function is to store sugars and other nutrients, although they also contribute to the radial strength of the tree (Burgert and Eckstein 2001). The fibers are long prismatic cells, often resembling a hexagon in cross-section, that provide mechanical support to the tree. For mechanical purposes, wood is considered an orthotropic material, the three axes of symmetry being the longitudinal (L, along the fibers), radial (R, along the rays), and tangential (T, across the rays) (see Fig. 1). In balsa, the vessels are about 380 μm in length and 200-350 μm in diameter, the rays are about 30 μm in length and 20-50 μm in cross-section, and the fibers are about 700 μm in length and 20-40 μm in diameter, decreasing with density. The thickness of the double cell wall is about 4 μm in vessels, 0.9 μm in rays, and between 0.8 μm and 3 μm in fibers, increasing with density (Easterling et al. 1982; Da Silva & Kyriakides 2007; Borrega et al. 2014).

The wood cell wall consists of a primary layer and three secondary layers, the S1, S2 and S3. The S2 is generally the thickest layer, making up about 80-90% of the total cell wall thickness in spruce tracheids (Fengel and Wegener 2003). In high density balsa, the S2 layer makes up about 73% of the cell wall thickness, while in low-density balsa the S2 is of similar thickness as the S1 and S3 layers, making up about 30% of the total cell wall thickness (Borrega et al. 2014). The middle lamella is a thin layer located between primary layers of adjacent cells, bonding them together.

The cell wall layers in woods are made up of lamellae having a fiber composite structure, in which cellulose microfibrils are embedded in a matrix of hemicelluloses and lignin. In the primary layer, the cellulose microfibrils have no definite orientation. In the secondary S1 and S3 layers, the microfibrils are oriented almost at 90° from the longitudinal cell axis, while in the S2 layer they are mostly aligned with the longitudinal axis, with angles typically varying between 10-30° (Barnett and Bonham 2004; Donaldson 2008). In balsa, the mean microfibril angle (MFA) appears to be less than 2°, irrespective of density (Borrega et al. 2014). The thickness and the low mean MFA of the S2 layer largely govern the axial mechanical properties of wood, particularly the stiffness (Cave 1969). The mechanical contribution of the S1 and S3 layers appears to be significant when wood is loaded in the transverse direction (Bergander and Salmén 2002).

Cellulose microfibrils in woods contain both crystalline and amorphous regions. The degree of crystallinity has been determined to be typically on the order of 40-60% for both softwoods and hardwoods (Andersson et al. 2004; Wikberg and Maunu 2004; Penttilä et al. 2013). In balsa, the degree of crystallinity appears to be much higher, about 80-90% (Borrega et al. 2014). The cellulose crystallites are about 3 nm in width and about 20-30 nm in length, much in agreement with values reported for other woods (Hori et al. 2002; Peura et al. 2008; Penttilä et al. 2013; Borrega et al. 2014). The crystalline structure of cellulose dominates the axial mechanical properties of wood, while the ligno-hemicellulosic matrix appears to have a more pronounced effect on the transverse mechanical properties (Bergander and Salmén 2002).

Materials and methods

Balsa wood

End-grain balsa blocks with dimensions 50 x 50 mm^2 in cross-section and 300 mm in length were obtained from National Balsa Wood Co. and Specialized Balsa Wood LLC. In addition, end-grain balsa sheets with dimensions 76 mm in thickness, 610 mm in width and 1219 mm in length were delivered by Baltek®. The sheets were composed of small blocks, up to 100 x 100 mm^2 in cross-section, glued together. The equilibrium moisture content of the wood at room ambient conditions, determined by oven-drying representative samples at 103 °C for 24 hours, was 5.8 ± 1.2%. At this moisture content, the density of individual blocks varied from 60 to 380 kg/m^3. Balsa specimens of different densities were produced for mechanical testing. Specimens with densities below 100 kg/m^3, between 100-200 kg/m^3, and above 200 kg/m^3 are here denoted as low density (LD), medium density (MD) and high density (HD) balsa, respectively.

Mechanical testing

Axial and radial compression

Rectangular balsa specimens with dimensions 13 x 13 mm^2 in cross-section and 50 mm in length were tested in compression; the length corresponded to the axial or radial direction in wood. The specimens were compressed in an Instron 4201, equipped with a 5kN load-cell, under displacement control. The displacement rate of the cross-head was set to 2 mm/s in axial compression and 1 mm/s in radial compression. An Instron 2630-104 extensometer was used to measure the compressive displacement at the specimen's mid-length. The load and displacement were recorded, and the stress, strain and Young's modulus were calculated. For those specimens that exhibited a drop in stress after plastic yielding, the compressive strength was determined as the maximum stress. Most LD balsa specimens in axial compression and those specimens tested in radial compression did not exhibit a clear drop in stress, but rather the stress transitioned into a plateau during the plastic regime. In such cases, the strength was determined as the stress at a strain offset of 0.2%.

An additional set of LD and HD balsa specimens, having a notch on one side at about mid-length, was tested in axial and radial compression. The notch did not affect the crushing strength of the specimens, and it only served to initiate failure away from the compression platens. Here, the strain was not measured with an extensometer, but it was

only approximated as the ratio of the cross-head displacement over the length of the specimen. These particular specimens were used to examine the mode of failure in compression (see below).

Bending

Balsa beams with dimensions 13 x 13 mm^2 in cross-section and 204 mm in length were tested in three-point bending, with a loading span of 170 mm. The bending tests were conducted in an Instron 4201, equipped with a 500 N load-cell, under displacement control. The displacement rate of the cross-head was set to 2 mm/s, and the deflection of the beams was measured with a Trans-Tek 240 Series linear voltage displacement transducer (LVDT). From the recorded load and displacement data, the bending stress and strain, modulus of elasticity (MOE) and modulus of rupture (MOR) were calculated. The MOR is a measure of the bending stress at fracture, calculated by assuming linear elasticity up to fracture.

Torsion

Round balsa specimens with dimensions 36 mm in diameter and 300 mm in length were prepared with a lathe. The middle section of the rods was then further reduced to about 22 mm in diameter, to ensure that failure developed away from the gripping clamps. Furthermore, to avoid crushing the wood while tightening the clamps, hexagonal end-caps made out of plywood were machined and glued with DAP Weldwood plastic resin to both ends of each balsa specimen.

Torsion tests were conducted in an Instron 1321, equipped with a 50 kN load-cell, under angular displacement control. The angular displacement rate of one of the clamps was set to 0.5°/s, while the other clamp remained stationary. Two metallic cubes were glued to the middle section of the balsa specimens, about 60-90 mm apart, and two LVDTs were used to measure the linear displacement of the cubes during torsion. The linear displacement was then converted to angular displacement, based on a preset calibration done at the beginning of each test. From the recorded torque and angular displacement data, the shear stress, strain, and modulus were calculated.

Scanning electron microscopy

After the mechanical tests, sections containing the failure zone were cut out from selected LD and HD balsa specimens, and the mode of failure in compression, bending and torsion was examined in a JEOL JSM-6610LV scanning electron microscope (SEM). The surface layers in the sections were removed with an industrial razor blade to obtain better images in the SEM. All sections were observed without coating. Micrographs were taken using the secondary electron detector in the SEM, operated at an accelerating voltage of 5-20 kV and in low-vacuum (30 Pa) mode.

Nanoindentation

A small HD balsa (264 kg/m^3) cube was embedded in Spurr's resin and placed under vacuum for 48 hours to complete impregnation. Then, to produce a smooth surface for nanoindentation, thin sections across the grain were cut with an ultramicrotome (Leica Ultracut UCT) equipped with a diamond knife. After microtoming, the cube was glued to a metal shim and magnetically clamped to the sample stage of a Hysitron TriboIndenter system (Hysitron Inc., Minneapolis, USA). Images of the fiber cell walls were produced with the indenter tip by means of in situ scanning probe microscopy (SPM). From the SPM images, the indent positions were manually selected at about half-thickness of the cell wall. Nanoindentation experiments were performed with a Berkovich tip (a three-sided pyramid) in load-control mode, using a force of 100 μN. The three segments of the load-displacement curve were: loading in 10 s, holding time of 5 s, and unloading in 10 s. The hardness of the cell wall and the reduced elastic modulus, determined from the unloading curve, were calculated according to Oliver & Pharr (2004).

Nanoindentation experiments were also conducted on a LD balsa (75 kg/m^3) cube, after preparing the sample following the procedure described above. However, we were unable to obtain reliable data due to the small cell wall thickness relative to the indent size, even at loads as low as 15 μN. For this reason, only those results from nanoindentation on HD balsa will be reported.

Results and discussion

Axial compression

Axial compression is one of the main loading modes of balsa wood in structural sandwich panels. Typical stress-strain curves in axial compression for LD (71 kg/m^3) and HD (265 kg/m^3) balsa specimens are shown in Fig. 2. The stress-strain curves showed an initial linear elastic response, followed by non-linear plastic yielding. Once the maximum stress (compressive strength) was reached, the evolution of the stress was dependent on the wood density. In LD balsa, the stress transitioned smoothly into a plateau, while in HD balsa the stress dropped abruptly and then increased again until it seemingly reached a plateau (Fig. 2). The drop in stress and the subsequent transition to a plateau were more pronounced in balsa specimens of higher density. The axial compressive response of balsa observed in this study is similar to that reported by Easterling et al. (1982) and Da Silva & Kyriakides (2007).

The axial Young's modulus and compressive strength of balsa increased linearly with density, reaching values up to 9 GPa for the modulus and 43 MPa for the strength (Fig. 3). The data for the modulus showed some scatter at the highest densities, and thus the goodness of the linear fit was lower than in the case of strength. By extrapolating the linear fits up to a density equivalent to the density of the wood cell wall, one may obtain a measure of the axial cell-wall properties. The dry density of the cell wall is about 1469 kg/m^3 in all woods (Kellogg and Wangaard 1969), and considering that the moisture content of balsa at the time of testing was about 6%, the density of the cell wall was calculated to be 1557 kg/m^3. Substituting this density into the linear fit equations in Fig. 3 gave an axial Young's modulus and compressive strength for the cell wall of 41 GPa and 185 MPa, respectively.

The axial elastic modulus in wood is strongly dependent on the MFA in the S2 layer of the cell wall. For MFAs smaller than 10°, the axial cell-wall modulus, extrapolated from tensile experiments of *Pinus radiata* samples, appears to be around 40 GPa (Cave 1969). In balsa, the mean MFA is less than 2° (see Borrega et al. 2014), and thus the axial cell-wall modulus extrapolated here (41 GPa) is in agreement with the modulus reported by Cave (1969). The extrapolated axial cell-wall compressive strength (185 MPa) is similar to the values of 190-200 MPa estimated from compression data of balsa by Vural & Ravichandran (2003) and Da Silva & Kyriakides (2007). These strength values are somewhat higher than the 125-160 MPa measured from direct compression of cell wall

micropillars in spruce, Keranji and Loblolly pine fibers (Zhang et al. 2010; Adusumalli et al. 2010). Artifacts produced during FIB milling as well as dimensional variations in the cross-section of the micropillars might explain their lower compressive strength values.

The cellular structure in balsa wood is mostly composed of fibers; their volume fraction is between 66-76% (Borrega et al. 2014). Fibers are long prismatic cells with a somewhat hexagonal cross-section. If the cellular structure in balsa is idealized to resemble a honeycomb, that deforms and then yields uniaxially, then the axial Young's modulus (E_A^*) and compressive strength (σ_A^*) can be calculated as:

$$E_A^* = E_S \left(\frac{\rho^*}{\rho_S}\right) \quad (1)$$

$$\sigma_A^* = \sigma_S \left(\frac{\rho^*}{\rho_S}\right) \quad (2)$$

where E_S and σ_S are the axial cell-wall modulus (41 GPa) and compressive strength (185 MPa), and ρ^* and ρ_s are the density of balsa and the density of the wood cell wall (1557 kg/m^3), respectively (Gibson and Ashby 1997). The model from Eq. 1, plotted in Fig. 3a, showed a good agreement with the linear fit determined experimentally. The model from Eq. 2, plotted in Fig. 3b, seemed to slightly overestimate the compressive strength as a function of density. This may due to the fact that the cellular structure in balsa (and in woods) does not only consist of fibers, but other types of cells such as rays and vessels exist. Therefore, at a given density, the fibers in balsa wood carry a higher share of the load than the cells in a honeycomb. It is also possible that uniaxial plastic collapse of fibers is not the only failure mechanism in axial compression, but other mechanisms are involved.

The failure mechanisms in axial compression were examined in detail from selected LD (71 kg/m^3) and HD (265 kg/m^3) balsa specimens. These specimens were compressed either up to failure (crushing strength) or up to 8-10% strain After the compression tests, the failure zone in the specimens was examined in the SEM. In LD balsa, failure was initiated by local buckling followed by folding of the fiber cell walls (Figs. 4a,b), in agreement with observations by Vural & Ravichandran (2003) and Da Silva & Kyriakides (2007). After failure, the stress remained constant with increasing compressive strain (see Fig. 2). During this stage, concertina folding developed in the cell

walls, and the failure band increased in size as neighboring fibers were crushed (Figs. 4c,d). The rest of the structure, away from the failure band, appeared to remain intact.

During axial compression of all but dense honeycombs, failure by simple plastic collapse seldom occurs because the limiting stress for plastic buckling of the cell walls tends to be reached first (Gibson and Ashby 1997). According to Wierzbicki (1983), the stress required for axial collapse by plastic buckling (σ_{pb}^{*}) can be calculated as:

$$\sigma_{pb}^{*} = m\,\sigma_S \left(\frac{\rho^{*}}{\rho_S}\right)^{\frac{5}{3}} \qquad (3)$$

where m is a factor that takes into account the uniformity of the cell wall thickness. For regular hexagons with uniform wall thickness, m equals to 5.6 (Gibson and Ashby 1997). In wood, the fibers are not regular hexagons, and the thickness of the cell wall is not uniform. A value of 3.5 was used in this study to fit the model from Eq. 3 to the axial compressive strength data of LD and MD balsa. As shown in Fig. 3b, plastic buckling may be a potential failure mechanism in axial compression of balsa with densities lower than 200 kg/m^3, in agreement with the SEM observations in Fig. 4 and with results reported by Vural & Ravichandran (2003).

The SEM examination of HD balsa specimens revealed that failure in axial compression was initiated by buckling, followed by tangential displacement of the buckled fibers (Figs. 5a,b). This type of failure, reminiscent of kink band formation, is facilitated by local misalignment of fibers due to the presence of rays, which leads to the development of shear stresses during compression (Vural and Ravichandran 2003; Da Silva and Kyriakides 2007). Some cell wall folding can also be observed in Fig. 5b. After failure, the compressive stress dropped by about 40% and then it slightly recovered with increasing strain (see Fig. 2). This stress-state corresponded to a progressive tangential displacement and crushing of the fibers, due to combined compression and shear forces. Some of the crushed fibers in the failure zone can be seen, in Figs. 5c and d, oriented at about 90° from their initial alignment. Similarly to LD balsa, the rest of the wood structure away from the failure band appeared to remain intact.

Failure by kink band formation during axial compression is a recognized mechanism in composites with fiber misalignment. Increasing the angle of fiber misalignment reduces

the compressive strength of the material due to increasing shearing forces between the fibers (Vural and Ravichandran 2003; Da Silva and Kyriakides 2007). The stress required for kink band formation (σ_{kb}^*) can be calculated, according to Budiansky & Fleck (1993), as:

$$\sigma_{kb}^* = \frac{G_A^*}{1+\theta/\gamma_y} \quad (4)$$

where G_A^* is the axial shear modulus of the material, θ is the angle misalignment and γ_y is the yield strain in longitudinal shear. In wood, the axial shear modulus and strength vary linearly with density (Gibson and Ashby 1997). Moreover, the axial cell-wall shear modulus (G_S) and strength (τ_S) in balsa wood equal to 2.1 GPa and 31 MPa, respectively (see torsion results below), thus giving a yield strain (γ_y) of 0.015, independent of density. Recently, we have reported the mean fiber misalignment in MD balsa to be 6.1° (Borrega et al. 2014), similar to misalignment angles measured by Da Silva & Kyriakides (2007). Substituting these values into Eq. 4, the stress required for kink band formation was computed and plotted as a function of density in Fig. 3b. It can be seen that balsa failed in axial compression at stresses much lower than those required for kink band formation. It is likely that the kink band formation observed in Figs. 5a,b was preceded by simple plastic collapse of the cell wall. It might also be possible that angles for fiber misalignment are closer to the 9° measured by Vural & Ravichandran (2003). In fact, at angles of 10°, the stresses required for kink band formation agreed well with the compressive strength data for densities higher than 200 kg/m^3 (model not shown).

Radial compression

The mechanical behavior of balsa in compression along the radial axis of symmetry (see Fig. 1) is discussed in this section. Stress-strain curves in radial compression of selected LD (88 kg/m^3) and HD (265 kg/m^3) balsa specimens are shown in Fig. 6. The stress-strain curves showed an initial linear elastic response, followed by non-linear plastic yielding. In LD balsa, the plastic deformation was accompanied by a plateau in the stress, while in HD balsa the stress increased slightly as deformation increased. The steeper slope of the stress-strain curve during plastic deformation in balsa wood of higher density has also been reported by Easterling et al. (1982) and Da Silva & Kyriakides (2007).

The radial Young's modulus and compressive strength of balsa increased with density, reaching values up to 0.5 GPa for the modulus and 3.8 MPa for the strength at the highest densities (Fig. 7). The radial modulus and strength were over an order of magnitude lower than in axial loading. Wood is weaker and more compliant when loaded in the transverse (radial or tangential) direction than in the axial direction. The reasons for this are found in the ultrastructure of the cell wall as well as in the cellular structure of wood. In transverse compression, the stiffness and strength of wood are lower because the cellulose microfibrils, which are the main load-bearing elements in the cell wall, are predominantly oriented perpendicular to the loading direction (Bergander and Salmén 2002; Salmén and Burgert 2009). Furthermore, the fibers are loaded perpendicular to their main axis, which results in bending of their cell walls, similar to the behavior of cells in a honeycomb when loaded in-plane (Easterling et al. 1982; Gibson and Ashby 1997). The transverse mechanical properties of wood are higher in the radial direction, compared to the tangential direction, due to the reinforcing effect of the rays.

To account for the effect of rays in radial loading, a simple rule of mixtures may be used to determine the radial Young's modulus (E_R^*) and strength (σ_R^*) in balsa wood:

$$E_R^* = V_r E_r^* + (1 - V_r) E_f^* \quad (5)$$

$$\sigma_R^* = V_r \sigma_r^* + (1 - V_r) \sigma_f^* \quad (6)$$

where V_r is the volume fraction of rays (V_r = 21.9%, see Appendix 1), E_r^* and σ_r^* are the modulus and compressive strength of the rays, and E_f^* and σ_f^* are the modulus and strength of the fibers (for simplicity, here we consider balsa to be made up of only rays and fibers). Rays are brick-like parenchyma cells with their main axis aligned along the radial direction in wood, while fibers are long prismatic cells with their main axis aligned along the axial direction. Therefore, during radial loading, the cell walls in rays are axially compressed but the cell walls in fibers bend. Then:

$$E_R^* = V_r E_{S_r} S_r + (1 - V_r) E_{S_f} \left(S_f\right)^3 \quad (7)$$

$$\sigma_R^* = V_r \sigma_{S_r} S_r + (1 - V_r) \sigma_{S_f} \left(S_f\right)^2 \quad (8)$$

where E_{Sr} and σ_{Sr} are the radial cell-wall modulus and compressive strength of rays, E_{Sf} and σ_{Sf} are the radial cell-wall modulus and compressive strength of fibers, S_r is the solid fraction of rays and S_f is the solid fraction of fibers. The solid fraction of rays and fibers appears to vary as a function of balsa density (see Appendix 1), and assuming that $E_{Sr} = E_{Sf}$ and $\sigma_{Sr} = \sigma_{Sf}$, Eqs. 7 and 8 are transformed into:

$$E_R^* = C_1 E_S \left(V_r S_r + (1 - V_r)(S_f)^3 \right) \quad (9)$$

$$\sigma_R^* = C_2 \sigma_S \left(V_r S_r + (1 - V_r)(S_f)^2 \right) \quad (10)$$

where E_S and σ_S are the axial cell-wall modulus (41 GPa) and compressive strength (185 MPa), and C_1 and C_2 are coefficients that account for the anisotropy of the wood cell wall. By fitting Eqs. 9 and 10 to the experimental data in Fig. 7, and extrapolating up to a density of 1557 kg/m^3, radial cell-wall properties of 9.2 GPa (C_1=0.22) for modulus and 36 MPa (C_2=0.19) for strength were obtained. These cell-wall properties are lower than the 19 GPa for modulus and 50 MPa for strength extrapolated by Gibson and Ashby (1997). However, those authors did not consider the effect of the rays in extrapolating the radial properties of the cell wall. The radial cell-wall modulus extrapolated here (9.2 GPa) agrees well with previous studies suggesting that the transverse cell-wall modulus in wood is lower than 10 GPa (Cave 1969; Salmén 2004).

The contribution of rays and fibers to the radial Young's modulus and compressive strength in balsa is shown in Fig. 7. The models from Eq. 9 and 10 seemed to slightly underestimate the radial mechanical properties, but nonetheless they showed a rather good agreement with the experimental data. It appears from Fig. 7a that rays have a higher contribution than fibers to the radial modulus of balsa wood, while rays have a higher contribution to the strength only at densities below 200 kg/m^3 (Fig. 7b).

The mode of failure in radial loading was examined in the SEM for selected LD (88 kg/m^3) and HD (265 kg/m^3) balsa specimens. The specimens were compressed either up to failure (compressive strength) or up to 8-10% strain. Failure in radial compression occurred, in both LD and HD balsa, by plastic collapse and subsequent flattening of the cell walls in fibers, but also in rays (Figs. 8a,b). After failure, the stress gradually transitioned into a plateau in LD balsa, while it appeared to increase slightly in HD balsa.

Along with increasing compression strain, wider areas of the balsa structure failed, and eventually the vessels collapsed (Figs. 8c,d). The progressive collapse of the cell walls resulted in densification of the structure, which was more evident in HD balsa than in LD due to the higher solid fraction of fibers in the former.

Bending

Bending experiments of wood are generally conducted as an alternative to tension tests, due to the easier preparation of test specimens. Furthermore, many structural wood products are subjected to bending, and thus data obtained from laboratory tests can be directly related to service conditions. The mechanical properties typically reported in bending are the modulus of elasticity (MOE) and the modulus of rupture (MOR). The MOE is not a true elastic modulus because shear deformation is ignored in the computation of total deformation during bending (Bodig and Jayne 1982). Moreover, the MOR is computed under the assumption of linear elastic behavior and thus it cannot be used to predict the ultimate failure stress of a composite. Nonetheless, the MOE and MOR are widely used in characterizing the mechanical properties of wood in bending.

Typical force-displacement curves in bending of LD (88 kg/m^3) and HD (227 kg/m^3) balsa specimens are shown in Fig. 9. A force-displacement curve is shown instead of a stress-strain curve because the stress and strain in bending vary throughout the beam. The bending response of balsa was linear-elastic up to the proportional limit. Beyond this point, the material started yielding plastically until it fractured at a flexural stress corresponding to the MOR. The plastic yielding appeared to be more pronounced in balsa wood of higher density (see Fig. 9). The MOE and MOR of balsa increased linearly with density, with values up to 8 GPa for MOE and 70 MPa for MOR at the highest densities (Fig. 10). The linear dependence of these properties on density was expected because in bending, wood fibers on the lower part of the beam are axially extended until they eventually fail due to tension stresses. The extrapolation of MOE and MOR values up to a density of 1557 kg/m^3 gave cell-wall properties of 36 GPa for MOE and 320 MPa for MOR. The cell-wall MOE was a good approximation to the 41 GPa extrapolated for the axial cell-wall modulus (E_S) in Fig. 4a, given that in wood beams with a span-to-depth ratio of 13 the MOE is about 0.9 times the axial modulus (Bodig and Jayne 1982). The

320 MPa for cell-wall MOR is within the range of 300-400 MPa reported by Cave (1969) for tensile cell-wall strength in pine wood samples.

If the cellular structure in balsa is idealized to resemble a honeycomb, then the MOE and MOR can be calculated as:

$$MOE^* = C_3 E_S \left(\frac{\rho^*}{\rho_S}\right) \quad (11)$$

$$MOR^* = C_4 \sigma_S \left(\frac{\rho^*}{\rho_S}\right) \quad (12)$$

where E_S and σ_S are the axial cell-wall modulus (41 GPa) and compressive strength (185 MPa), and C_3 and C_4 are factors related to the different compression and tension values in composite materials. By assuming the extrapolated values from the linear fits in Fig. 10, then C_3 in Eq. 11 equals to 0.88 and C_4 in Eq. 12 equals to 1.73. The model from Eq. 11 agrees well with the experimental data for MOE (Fig. 10a), while the model from Eq. 12 appears to overestimate the MOR (Fig. 10b), similar to the model from Eq. 2 overestimating the axial compressive strength in Fig. 3b. As mentioned above, the balsa structure is not only composed of fibers, as idealized in a honeycomb, but other types of cells like rays and vessels exist. Therefore, at a given density, the fibers must carry a higher share of the load than if they were the sole cell type. It appears from Fig. 10 (and also from Fig. 3), that rays and vessels contribute more to the flexural (and axial) modulus than to the strength.

Failure of balsa specimens in bending occurred as the flexural stress corresponding to the MOR was reached on the bottom of the beam, subjected to tension, and the beam fractured. The fracture of selected LD (88 kg/m^3) and HD (227 kg/m^3) balsa specimens was examined in the SEM. The failure crack appeared to propagate across cells, rather than between cells (Fig. 11a). In LD balsa, the crack propagated rapidly across the depth of the beam, sometimes splitting it in two. In HD balsa, the propagation of the crack was somewhat more limited, and it was often hard to see the crack with a naked eye once the bending test had terminated. Although all specimens ultimately failed in tension, compressive failure occurred first. This is because wood is generally stronger in tension than in compression, and thus during bending, a maximum ultimate stress is first reached on the compression side (Bodig and Jayne 1982). Upon failure by compression, the

neutral plane moved towards the tension side, where wood ultimately failed and fractured. An example of compression failure during bending is shown in Fig. 11b, where the fibers in HD balsa are clearly seen to buckle, forming a failure band reminiscent of a kink band. This type is failure is similar to the failure observed during axial compression of HD balsa (see Figs. 5a,b).

Torsion

Along with axial compression, shear is one of the main loading modes of balsa wood in structural sandwich panels. Since torsion produces pure shear stress, torsion experiments were conducted in this study to investigate the shear behavior of balsa. Examples of stress-strain curves in torsion of LD (85 kg/m^3) and HD (240 kg/m^3) balsa specimens are shown in Fig. 12. The initial shear response of balsa was linear elastic, followed by a broad plastic deformation until failure occurred at about 2.5% strain. The shear modulus (G_A) and shear strength (τ_A) in torsion increased linearly with density, with values up to 0.55 GPa for modulus and 7 MPa for strength at the highest densities (Fig. 13). The shear modulus and strength values obtained here were found to be higher than those determined by Da Silva & Kyriakides (2007). Those authors, however, used a different experimental setup in order to determine the shear properties of balsa in both the axial-tangential and axial-radial plane. The extrapolation of the linear fits in Fig. 13, up to a density of 1557 kg/m^3, gave a shear cell-wall modulus of 2.1 GPa and shear cell-wall strength of 31 MPa. These values are similar to the out-of-plane (axial-radial or axial-tangential) shear modulus (2.6 GPa) and strength (30 MPa) extrapolated by Gibson & Ashby (1997).

If the cellular structure in balsa is idealized to resemble a honeycomb, the out-of-plane shear modulus G_A and strength (τ_A) may be calculated as:

$$G_A^* = C_5 E_S \left(\frac{\rho^*}{\rho_S}\right) \tag{13}$$

$$\tau_A^* = C_6 \sigma_S \left(\frac{\rho^*}{\rho_S}\right) \tag{14}$$

where E_S and σ_S are the axial cell-wall modulus (41 GPa) and crushing strength (185 MPa), and C_5 and C_6 are factors related to the cell geometry that are generally found from fits to data (Gibson and Ashby 1997). The value of C_5 was estimated to be 0.05, so the

product C_5E_S would correspond to the extrapolated shear cell wall modulus (G_S = 2.1 GPa). The value of C_6 was estimated to be about 0.17, so the product $C_6\sigma_S$ would correspond to the extrapolated shear cell-wall strength (τ_S = 31 MPa). As seen in Fig. 13, the models from Eq. 13 and 14 showed an excellent agreement with the experimental data, indicating that balsa subjected to torsion can be modeled as a honeycomb. Because the relative density does not only include the contribution of fibers, but also that of rays and vessels, it may be concluded that the whole cellular structure in balsa affects its shear properties.

Failure of balsa specimens during torsion occurred by fracture along the axial direction. Selected micrographs of LD (85-88 kg/m^3) and HD (219-239 kg/m^3) balsa specimens after fracture are shown in Figs. 14 and 15. In 3 out of 4 LD balsa specimens, the failure crack propagated according to a TR mode, where the first letter indicates the direction normal to the crack plane, and the second describes the direction of the crack propagation. This mode of crack propagation in LD balsa can be clearly seen in Figs. 14. In the remaining LD balsa specimen, as well as in 4 out of 5 HD balsa specimens, the crack propagated according to a RT mode (Figs. 15). The crack in the fifth HD balsa propagated in a mixed TR/RT mode. Previous results by Da Silva & Kyriakides (2007) showed that balsa was generally stronger in shear in the axial-radial plane, compared to the axial-tangential plane, and that the difference in shear properties between planes became more pronounced with increasing density. It is then likely that, in HD balsa, the crack tended to propagate along the weaker (tangential) direction. It may be also possible that, in LD balsa, the predominant direction (radial) for crack propagation was only coincidental. Testing a higher number of LD and HD balsa specimens would be needed to better elucidate on the predominant direction of crack propagation in balsa during torsion.

In addition to different modes of crack propagation, the fracture of torsion specimens also differed between LD and HD balsa. In LD balsa, the crack could clearly be seen with a naked eye, while in HD balsa the crack was rather difficult to see, even with the aid of the SEM. A closer examination of the fracture zone in LD balsa appeared to reveal that the crack mostly developed through the ray pockets, pulling apart individual cells (inter-cell propagation) (Fig. 14). In HD balsa, however, the crack seemed to propagate through the

cell walls (intra-cell) in fibers, but possibly also in rays (Fig. 15). This is somewhat surprising because in LD balsa the rays are denser than the fibers, while in HD balsa the fibers are considerably denser than the rays (see Borrega et al. 2014). Therefore, one might expect that the propagation of the crack would be intra-cell in LD balsa but inter-cell in HD balsa. The reasons for a predominant fracture behavior in balsa samples of different density, as observed in this study, are not yet fully understood.

Nanoindentation

The reduced modulus and hardness of the wood cell wall can be determined by nanoindentation. With this technique, a small indenter is driven into the cell wall, and the force and area of the indent are measured. The hardness is calculated from the area under the maximum load applied, while the reduced elastic modulus is calculated from the unloading section of the load-displacement curve (see Oliver and Pharr (2004) and Gindl and Schöberl (2004)). In HD balsa (264 kg/m^3), the mean cell-wall hardness and reduced modulus were 0.57 ± 0.11 and 19.4 ± 4.4 GPa, respectively. These values are mostly in agreement with the 0.40-0.56 GPa for hardness and 16-24 GPa for reduced modulus reported for 10 different hardwoods (Wu et al. 2009) and for spruce wood tracheids with mean MFAs close to 0° (Gindl et al. 2004). However, the reduced modulus determined by nanoindentation (19.4 GPa) is about half the value of the axial cell-wall Young's modulus (41 GPa) determined by extrapolation in axial compression experiments (see Fig. 3). It is generally recognized that nanoindentation is not a suitable technique to determine the axial elastic modulus of the wood cell wall because nanoindentation theory is based on the assumption of isotropy, which cannot be applied to wood due to the composite nature of the cell wall. Furthermore, for indents are performed with a Berkovich tip, a three-sided pyramid, the cellulose microfibrils in the cell wall are loaded at an angle of 25°, which obviously underestimates the axial elastic modulus (Gindl and Schöberl 2004).

Summary and conclusions

The mechanical properties of balsa wood in axial and radial compression, bending and torsion were investigated as a function of density. The density of balsa varied roughly from 60 to 380 kg/m^3. In axial compression, the Young's modulus and strength increased

linearly with density, reaching values up to 9 GPa for the modulus and 43 MPa for the strength at the highest densities. The main failure mechanism in LD balsa was plastic buckling, while failure in HD balsa probably occurred by a combination of plastic collapse and kink band formation. In radial compression, the Young's modulus and strength increased nonlinearly with density, and were over an order of magnitude lower than in axial compression, with values around 0.5 GPa for the modulus and 3.8 MPa for the strength at the highest densities. The radial mechanical properties were dependent on the fibers, which were subjected to bending, and on the rays, which were axially compressed during radial loading. Therefore, the radial modulus and strength increased with the sum of the fiber and ray contributions: with the cube and the square of the relative density of fibers, and linearly as a function of the relative density of rays, respectively. Failure occurred by plastic collapse of the cell walls in fibers and rays, resulting in densification of the structure.

In bending, the modulus of elasticity (MOE) and modulus of rupture (MOR) increased linearly with density, reaching values up to 8 GPa for MOE and 70 MPa for MOR at the highest densities. Failure occurred first on the upper side of the beam, subjected to compression, but the wood ultimately fractured on the lower side of the beam due to increased tensile stresses. In LD balsa, the crack propagated across the cell walls, largely through the whole depth of the beam. In HD balsa, the propagation of the crack was more limited, and often difficult to observe with a naked eye. Compression failure in HD balsa occurred as the fibers buckled and were laterally displaced, similar to the failure mechanism observed during axial compression.

In torsion, the shear modulus and strength increased linearly with density, reaching values up to 0.55 GPa for modulus and 7 MPa for strength at the highest densities. Failure occurred by fracture along the axial-radial or axial-tangential planes. The predominant mode of crack propagation seemingly differed between LD and HD balsa. In LD balsa, the crack tended to propagate between cells (inter-cell), along the radial direction and through the rays pockets. In HD balsa, the crack appeared to propagate across cells (intra-cells) and along the tangential direction in wood, splitting apart the fiber cell walls. The predominant mode of crack propagation in HD balsa might be related to the reinforcing effect that the rays exert in the radial direction.

The mechanical behavior of balsa was modeled by considering its cellular structure to resemble a honeycomb. In axial compression and bending, and particularly in torsion, the mechanical models showed a good agreement to the experimental data. However, the axial compressive strength and MOR were slightly overestimated, possibly due to the fact that the cellular structure in balsa (and in woods) does not only consist of fibers, but other type of cells such as rays and vessels exist. Fibers are the main load-bearing cells in wood. Therefore, at a given density, individual fibers in balsa were likely to carry a higher share of the load than individual cells in a honeycomb. In radial compression, a rule of mixtures was used to account for the contribution of rays to the radial modulus and strength of balsa wood. The resulting models showed a rather good agreement to the experimental data, even if the mechanical properties were slightly underestimated. However, the mechanical models in radial compression were limited by the current knowledge on the variation in volume and solid fraction of rays with balsa density, as well as on cell-wall properties in rays and fibers.

The mechanical properties of the wood cell wall were determined by extrapolating the mechanical properties of balsa up to a density equivalent to that of the solid cell wall (1557 kg/m^3 for a moisture content about 6%). In axial compression, the extrapolated cell-wall values were 41 GPa for Young's modulus and 185 MPa for strength, while in radial compression the extrapolated cell-wall modulus and strength were 9 GPa and 36 MPa, respectively. In bending, the extrapolated cell-wall MOE and MOR were 36 GPa and 320 MPa, respectively. The cell-wall MOE was a good approximation to the 41 GPa extrapolated for the axial cell-wall modulus, considering the relatively short span-to-depth ratio of balsa specimens used in the bending tests. In torsion, the extrapolated cell-wall shear modulus and strength were 2.1 GPa and 31 MPa, respectively. The axial cell-wall modulus and hardness were also determined by nanoindentation; in HD balsa, values of about 19 GPa for the modulus and 0. 57 for hardness were obtained. This cell-wall modulus was about half of that extrapolated (41 GPa) from mechanical tests of balsa, most likely due to the fact that, in an orthotropic material like wood, nanoindentation measures a combination of property values in the different directions.

Acknowledgements

Funding provided by BASF through the North American Center for Research on Advanced Materials (Program Manager Dr. Marc Schroeder; Dr. Holger Ruckdaeschel and Dr. Rene Arbterx) is gratefully acknowledged. The Hobby Shop in MIT is thanked for their help in preparing the balsa wood specimens for mechanical testing. Mike Tarkanian (MIT) is thanked for his help in planning the torsion tests. Dr. Alan Schwartzman (MIT) is thanked for his kind support with the nanoindentation experiments. Patrick Dixon (MIT) is thanked for his help in conducting the mechanical tests and discussing the results.

References

Adusumalli R-B, Raghavan R, Ghisleni R, Zimmermann T, Michler J (2010) Deformation and failure mechanism of secondary cell wall in Spruce late wood. Appl Phys A 100:447–452.

Andersson S, Wikberg H, Pesonen E, Maunu SL, Serimaa R (2004) Studies of crystallinity of Scots pine and Norway spruce cellulose. Trees - Struct Funct 18:346–353.

Barnett JR, Bonham VA (2004) Cellulose microfibril angle in the cell wall of wood fibres. Biol Rev 79:461–72.

Bergander A, Salmén L (2002) Cell wall properties and their effects on the mechanical properties of fibers. J Mater Sci 37:151–156.

Bodig J, Jayne BA (1982) Mechanics of wood and wood composites. 712p.

Borrega M, Ahvenainen P, Serimaa R, Gibson L (2014) Composition and structure of balsa (*Ochroma pyramidale*) wood. Submitted.

Budiansky B, Fleck NA (1993) Compressive failure of fibre composites. J Mech Phys Solids 41:183–211.

Burgert I, Eckstein D (2001) The tensile strength of isolated wood rays of beech (Fagus sylvatica L.) and its significance for the biomechanics of living trees. Trees 15:168–170.

Burgert I, Eder M, Frühmann K, et al. (2005) Properties of chemically and mechanically isolated fibres of spruce (*Picea abies* [L.] Karst.). Part 3: Mechanical characterisation. Holzforschung 59:354–357.

Cave ID (1969) The longitudinal Young's modulus of Pinus radiata. Wood Sci Technol 3:40–48.

Da Silva A, Kyriakides S (2007) Compressive response and failure of balsa wood. Int J Solids Struct 44:8685–8717.

Donaldson L (2008) Microfibril angle: Measurement, variation and relationships - A review. IAWA J 29:345–386.

Easterling KE, Harrysson R, Gibson LJ, Ashby MF (1982) On the mechanics of balsa and other woods. Proc R Soc London A 383:31–41.

Fengel D, Wegener G (2003) Wood. Chemistry, ultrastructure, reactions. 613p.

Fletcher MI (1951) Balsa—Production and utilization. Econ Bot 5:107–125.

Gibson LJ, Ashby MF (1997) Cellular Solids. Structure and properties, Second Ed. 510p.

Gindl W, Gupta HS, Schöberl T, et al. (2004) Mechanical properties of spruce wood cell walls by nanoindentation. Appl Phys A 79:2069–2073.

Gindl W, Schöberl T (2004) The significance of the elastic modulus of wood cell walls obtained from nanoindentation measurements. Compos Part A 35:1345–1349.

Hori R, Müller M, Watanabe U, Lichtenegger HC, Fratzl P, Sugiyama J (2002) The importance of seasonal differences in the cellulose microfibril angle in softwoods in determining acoustic properties. J Mater Sci 37:4279–4284.

Kellogg RM, Wangaard FF (1969) Variation in the cell-wall density of wood. Wood Fiber 1:180–204.

Oliver WC, Pharr GM (2004) Measurement of hardness and elastic modulus by instrumented indentation: Advances in understanding and refinements to methodology. J Mater Res 19:3–20.

Orso S, Wegst UGK, Arzt E (2006) The elastic modulus of spruce wood cell wall material measured by an in situ bending technique. J Mater Sci 41:5122–5126.

Penttilä PA, Kilpeläinen P, Tolonen L, Suuronen J-P, Sixta H, Willför S, Serimaa R (2013) Effects of pressurized hot water extraction on the nanoscale structure of birch sawdust. Cellulose 20:2335–2347.

Peura M, Müller M, Vainio U, Sarén M-P, Saranpää P, Serimaa R (2008) X-ray microdiffraction reveals the orientation of cellulose microfibrils and the size of cellulose crystallites in single Norway spruce tracheids. Trees - Struct Funct 22:49–61.

Salmén L (2004) Micromechanical understanding of the cell-wall structure. C R Biol 327:873–880.

Salmén L, Burgert I (2009) Cell wall features with regard to mechanical performance. A review. COST Action E35 2004–2008: Wood machining – micromechanics and fracture. Holzforschung 63:121–129.

Tze WTY, Wang S, Rials TG, et al. (2007) Nanoindentation of wood cell walls: Continuous stiffness and hardness measurements. Compos Part A Appl Sci Manuf 38:945–953.

Vural M, Ravichandran G (2003) Microstructural aspects and modeling of failure in naturally occurring porous composites. Mech Mater 35:523–536.

Wierzbicki T (1983) Crushing analysis of metal honeycombs. Int J Impact Eng 1:157–174.

Wikberg H, Maunu SL (2004) Characterisation of thermally modified hard- and softwoods by ^{13}C CPMAS NMR. Carbohydr Polym 58:461–466.

Wu Y, Wang S, Zhou D, et al. (2009) Use of nanoindentation and SilviScan to determine the mechanical properties of 10 hardwood species. Wood Fiber Sci 41:64–73.

Zhang X, Zhao Q, Wang S, Trejo R, Lara-Curzio L, Du G (2010) Characterizing strength and fracture of wood cell wall through uniaxial micro-compression test. Compos Part A Appl Sci Manuf 41:632–638.

Appendix 1.

The cellular structure of balsa mainly consists of fibers, rays and vessels. The dimensions, solid fraction and volume fraction of each type of cell in balsa wood of different densities have been determined by Borrega et al. (2014). Data for solid and volume fraction of rays are listed in Table A1.

Table A1. Mean solid and volume fraction of rays in balsa wood of different densities.

	LD balsa	MD balsa	HD balsa
*Balsa density, kg/m^3	64	163	274
Rays			
Solid fraction, %	6.5	7.4	8.3
Volume fraction, %	20.9	19.9	24.8

*Density determined at room conditions; moisture content of wood about 6%.

From the values in Table A1, the solid fraction of rays appears to increase only slightly as a function of density. However, the volume fraction of rays may be considered independent of wood density, the mean volume fraction being about 21.9%. Then, the density of balsa can be calculated as:

$$\rho_{balsa} = \rho_S\left(V_r S_r + (1 - V_r)S_f\right) \quad \text{(A1)}$$

where ρ_S is the density of the wood cell wall, V_r (21.9%) is the volume fraction of rays in balsa, S_r is the solid fraction of rays and S_f is the solid fraction of fibers (for simplificity, here we consider balsa to be made up of only rays and fibers). The dry density of the cell wall is about 1469 kg/m^3 in all woods (Kellogg & Wangaard 1969), and considering that the moisture content of balsa at room conditions was about 6%, the density of the cell wall (ρ_S) is about 1557 kg/m^3. Substituting into Eq. A1, S_f can be calculated for each of the measured balsa densities in Table A1.

The solid fraction of rays (S_r) and that of fibers (S_f) is plotted as a function of balsa density in Fig. A1. For $\rho_{balsa} = 0$, S_r and S_f equal to 0. For $\rho_{balsa} = \rho_S = 1557$ kg/m^3, one can assume that S_r and S_f equal to 1. As shown in Fig. A1, the volume fraction of rays and fibers as a function of wood density may be described by a polynomial function.

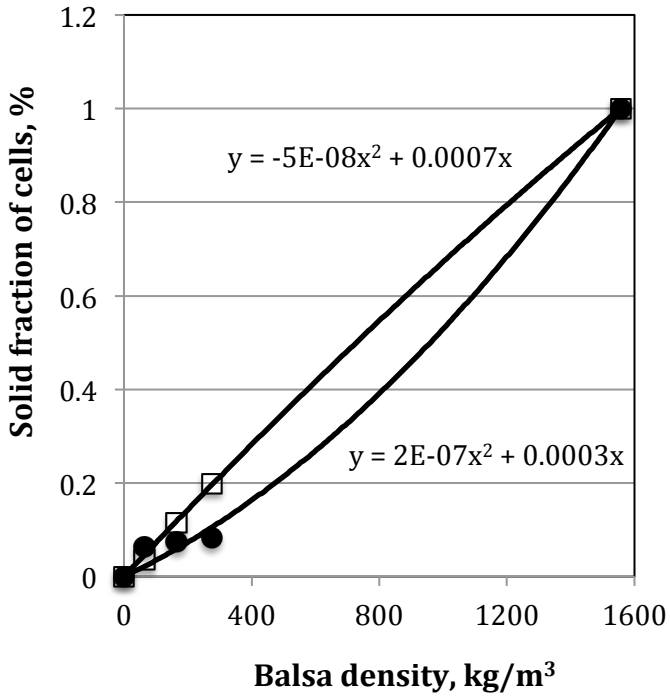

Fig. A1. Volume fraction of rays (circles) and fibers (squares) determined for different balsa densities. Black line and equation correspond to a polynomial fit to the data.

Figure captions

Fig. 1. SEM micrographs of balsa showing the main type of cells in (a) cross-section and (b) longitudinal view. L, R and T refer to the longitudinal, radial and tangential axes of symmetry.

Fig. 2. Stress-strain curves in axial compression tests of selected LD (71 kg/m^3) and HD (265 kg/m^3) balsa specimens. D and L in the x-axis refer to the displacement of the compression platen and to the length of the balsa specimen, respectively.

Fig. 3. (a) Axial Young's modulus and (b) compressive strength of balsa wood as a function of density. Solid black lines and equations correspond to linear fits to experimental data. Dashed black lines correspond to models (Eqs. 1 and 2) for modulus and strength. Red line in (b) corresponds to model (Eq. 3) for plastic buckling. Blue line in (b) corresponds to model (Eq. 4) for kink band formation.

Fig. 4. SEM micrographs of LD balsa showing (a and b) the initiation of failure by local buckling in axially crushed fibers (3.3% strain) and (c and d) the evolution of failure at 8.1% compressive strain.

Fig. 5. SEM micrographs of HD balsa showing (a and b) the initiation of failure by kink band formation in axially crushed fibers (3.3% strain) and (c and d) the evolution of failure at 10.1% compressive strain.

Fig. 6. Stress-strain curves in radial compression tests of selected LD (88 kg/m^3) and HD (265 kg/m^3) balsa specimens. D and L in the x-axis refer to the displacement of the compression platen and to the length of the balsa specimen, respectively.

Fig. 7. (a) Radial Young's modulus and (b) compressive strength of balsa wood as a function of density. Solid black lines correspond to polynomial fits to experimental data. Dashed black lines correspond to models (Eqs. 9 and 10) for modulus and strength. Red lines correspond to contribution of the rays, and blue lines correspond to contribution of fibers.

Fig. 8. SEM micrographs showing (a and b) cell collapse in LD balsa under radial loading (2.6% strain) and (c and d) the eventual collapse of vessels with increasing compressive strain, resulting in densification of the structure in (c) LD balsa (9.0% strain) and (d) HD balsa (9.5% strain).

Fig. 9. Force-displacement curves in bending tests of selected LD (88 kg/m^3) and HD (227 kg/m^3) balsa specimens.

Fig. 10. (a) Modulus of elasticity (MOE) and (b) modulus of rupture (MOR) of balsa wood as a function of density. Solid black lines and equations correspond to linear fits to

experimental data. Dashed black lines correspond to models (Eqs. 11 and 12) for MOE and MOR.

Fig. 11. SEM micrographs showing (a) the failure crack in bending propagating across cells on the tension side of LD balsa (0.7% strain) and (b) failure in bending by kink band formation on the compression side of HD balsa (1.1% strain).

Fig. 12. Stress-strain curves in torsion tests of selected LD (85 kg/m^3) and HD (240 kg/m^3) balsa specimens.

Fig. 13. (a) Shear modulus and (b) shear strength of balsa wood in torsion as a function of density. Solid black lines and equations correspond to linear fits to experimental data. Dashed black lines correspond to models (Eqs. 13 and 14) for shear modulus and strength.

Fig. 14. SEM micrographs of LD balsa (85-88 kg/m^3) after torsion showing the fracture crack in the axial-tangential plane (2.1% strain). The crack appears to be inter-cell, splitting the rays apart.

Fig. 15. SEM micrographs of HD balsa (219-239 kg/m^3) after torsion showing the fracture crack in the axial-radial plane (2.6% strain). The crack appears to be intra-cell, splitting the cell wall in fibers apart.

Fig. 1.

a)

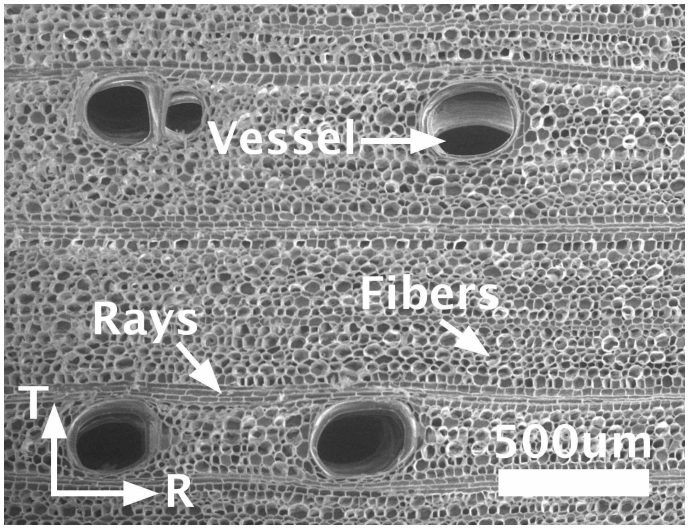

b)

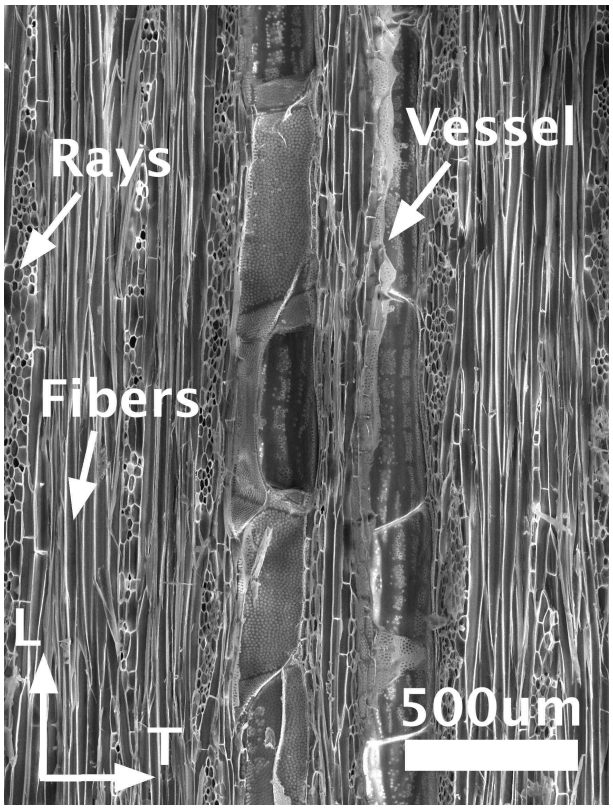

Fig. 2.

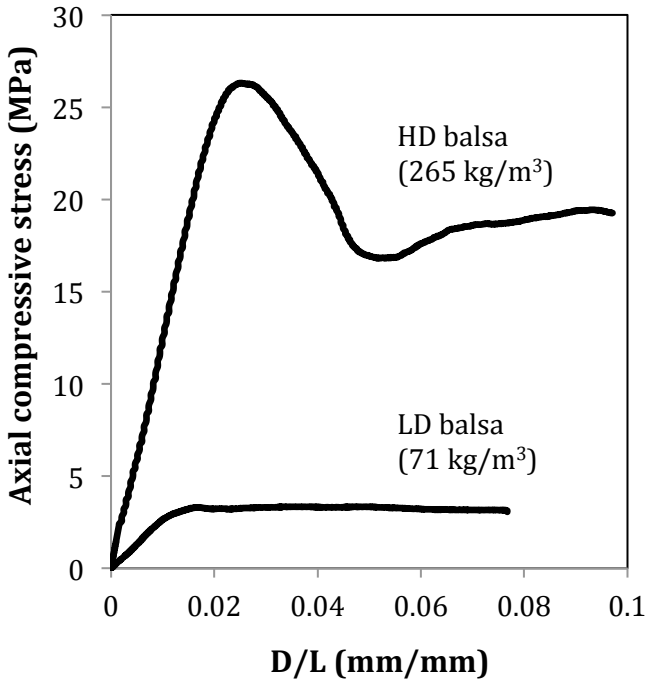
Axial compressive stress (MPa)
30
25
20
15
10
5
0
0
0.02
0.04
0.06
0.08
0.1
D/L (mm/mm)
HD balsa
(265 kg/m3)
LD balsa
(71 kg/m3)

Fig. 3.

a)

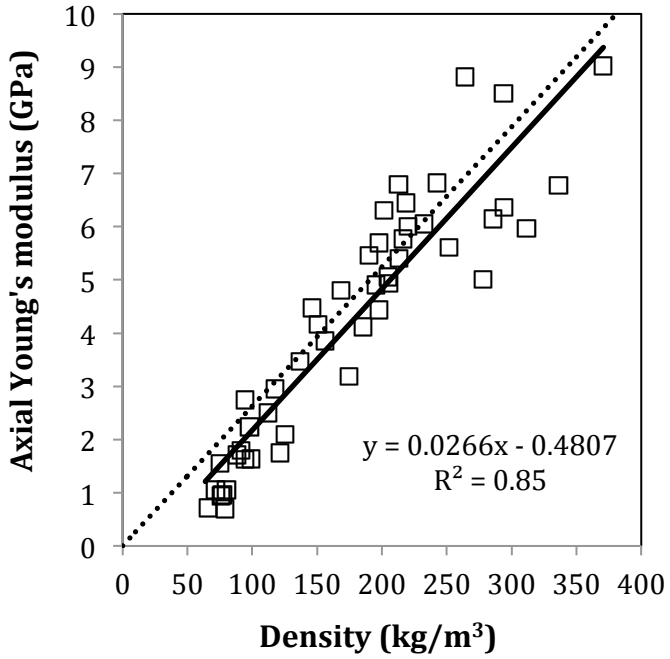
Axial Young's modulus (GPa)
Density (kg/m³)
y = 0.0266x - 0.4807
R² = 0.85

b)

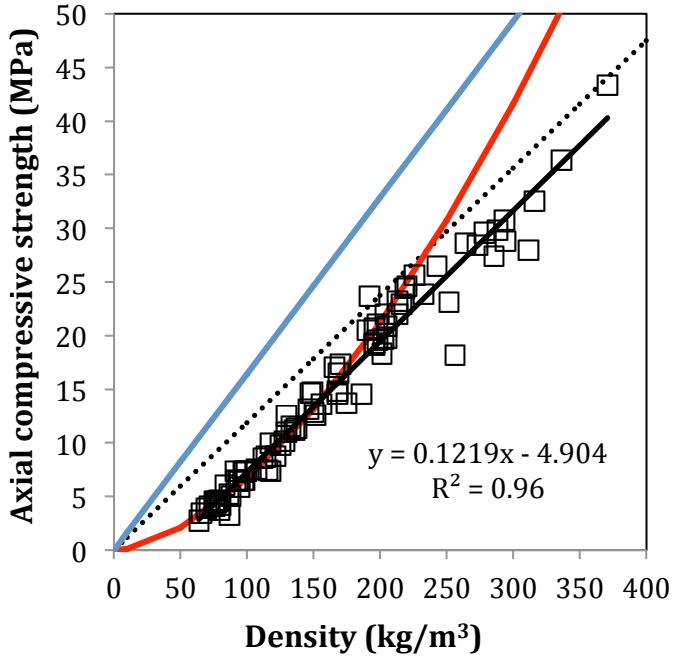
Axial compressive strength (MPa)
Density (kg/m³)
y = 0.1219x - 4.904
R² = 0.96

Fig. 4.

a)

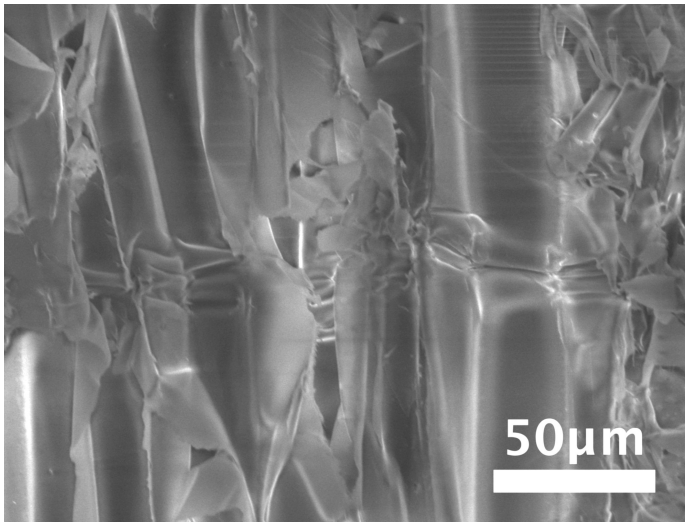

b)

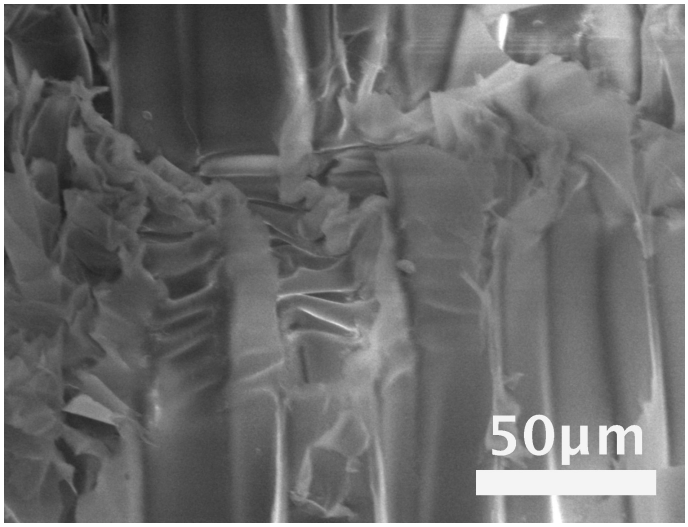

Fig. 4.

c)

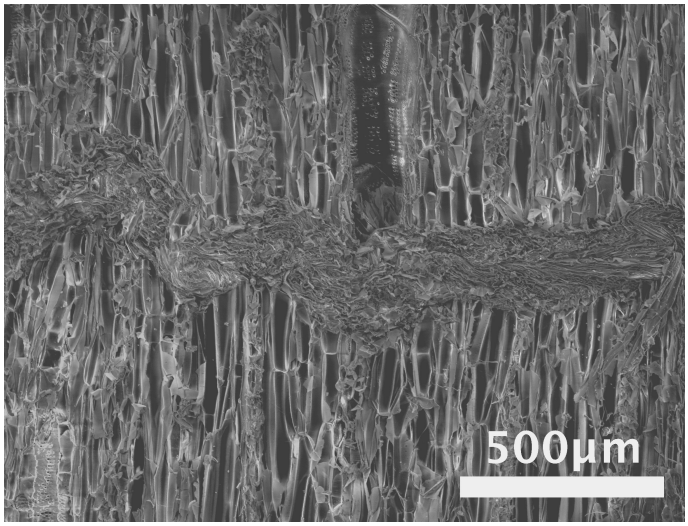

d)

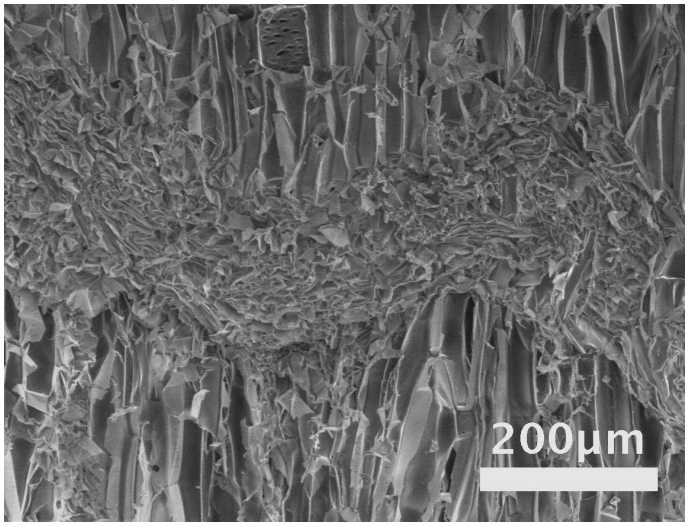

Fig. 5.

a)

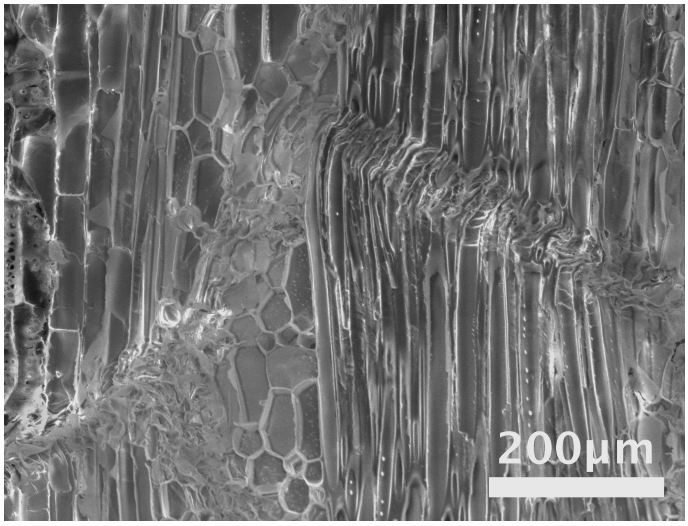

b)

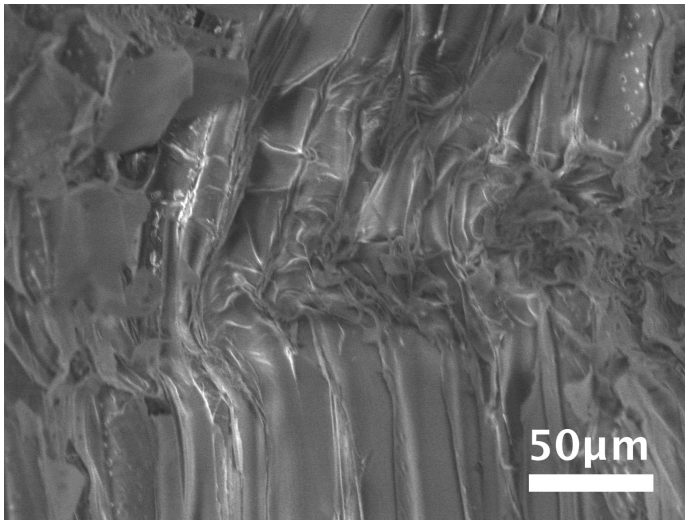

Fig. 5.

c)

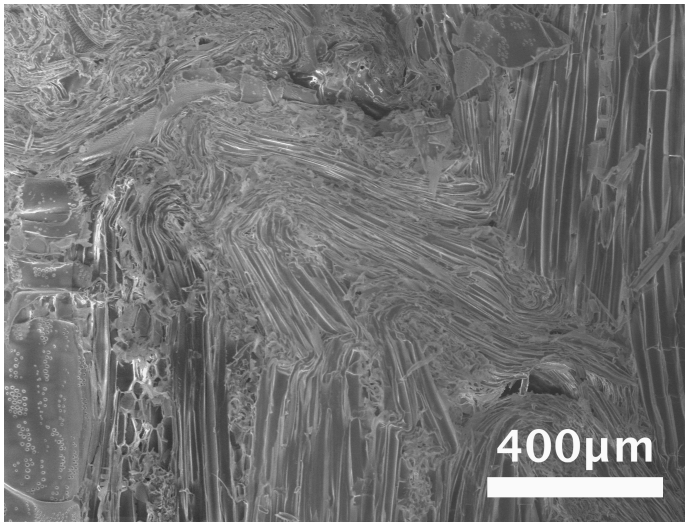

d)

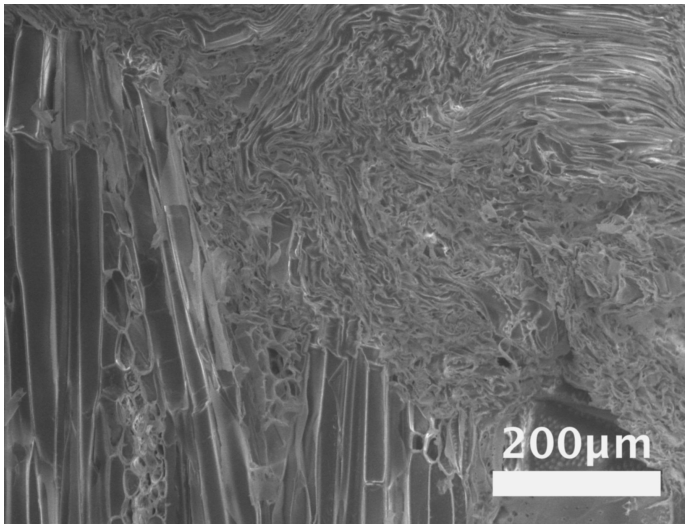

Fig. 6.

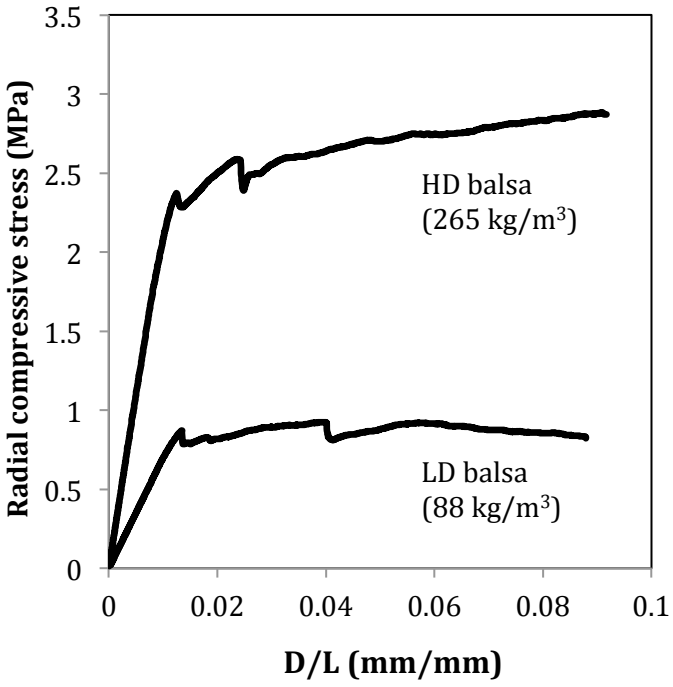
Radial compressive stress (MPa)
3.5
3
2.5
2
1.5
1
0.5
0
0
0.02
0.04
0.06
0.08
0.1
D/L (mm/mm)
HD balsa
(265 kg/m3)
LD balsa
(88 kg/m3)

Fig. 7.

a)

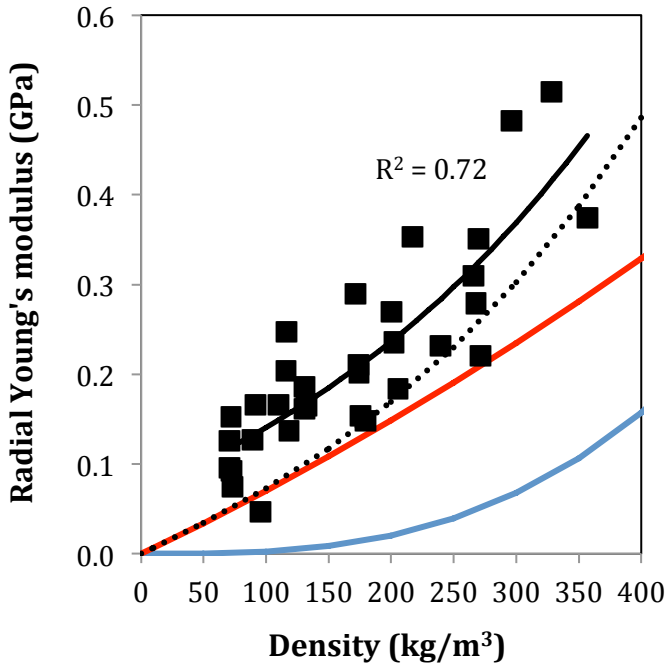
Radial Young's modulus (GPa)
0.6
0.5
0.4
0.3
0.2
0.1
0.0
R² = 0.72
0
50
100
150
200
250
300
350
400
Density (kg/m³)

b)

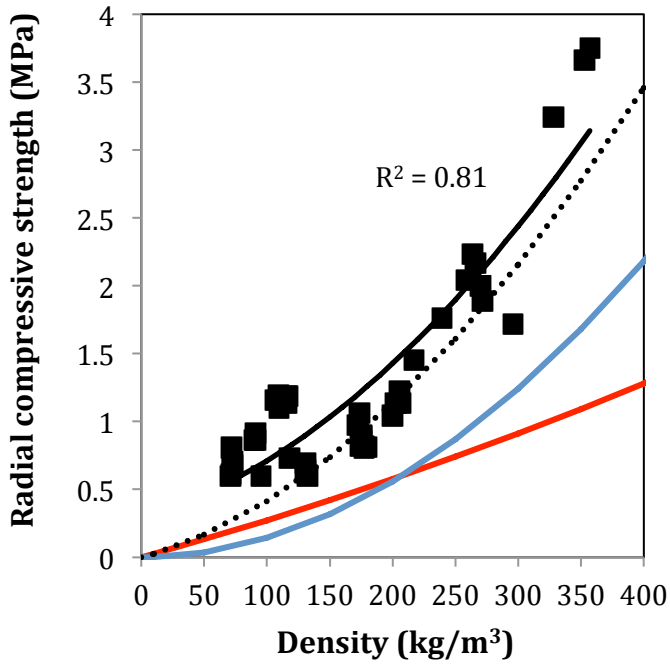
Radial compressive strength (MPa)
4
3.5
3
2.5
2
1.5
1
0.5
0
R² = 0.81
0
50
100
150
200
250
300
350
400
Density (kg/m³)

Fig. 8.

a)

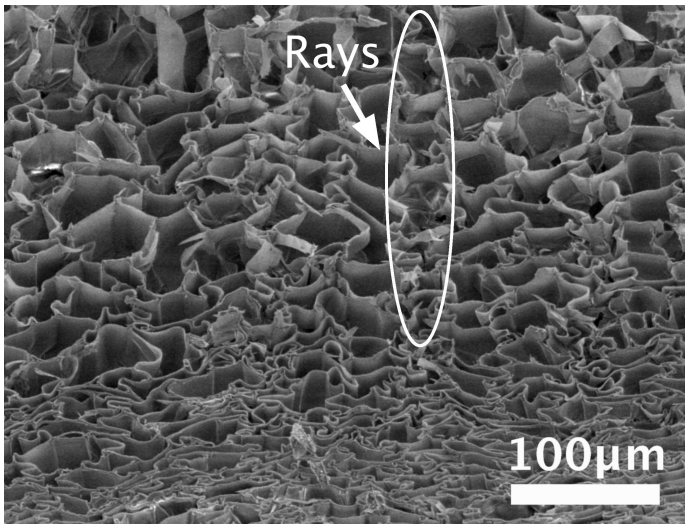

b)

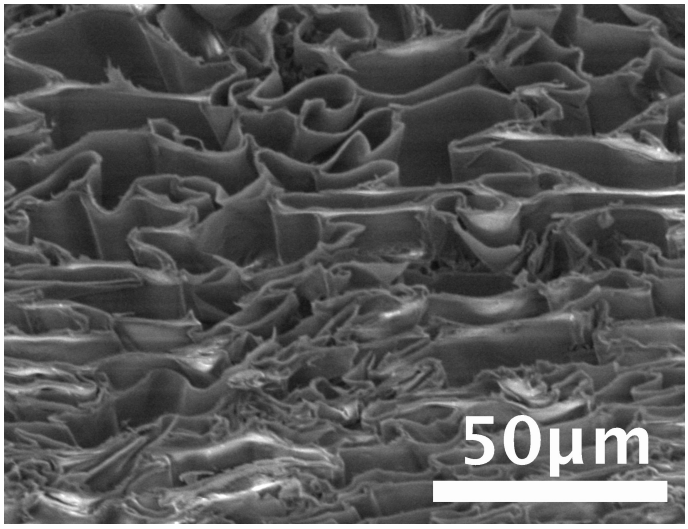

Fig. 8.

c)

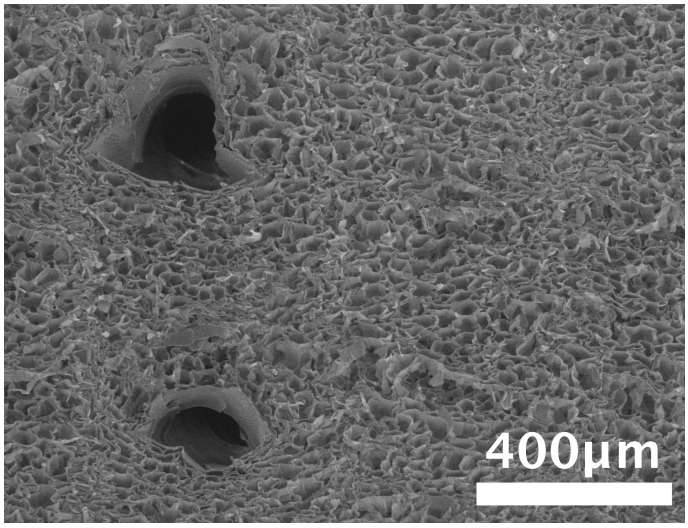

d)

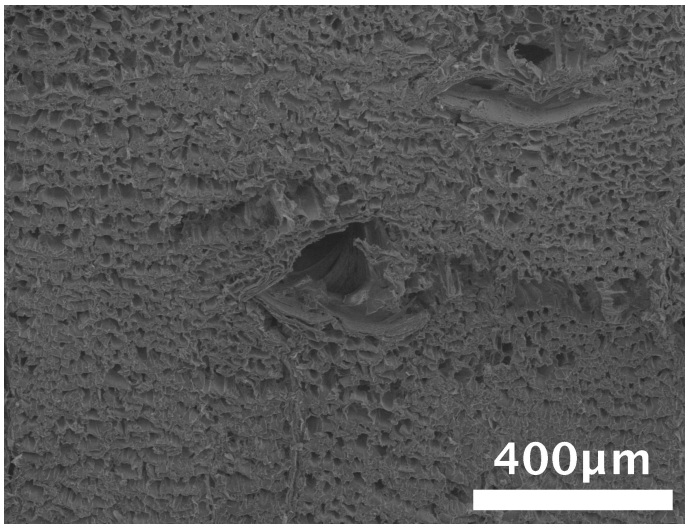

Fig. 9.

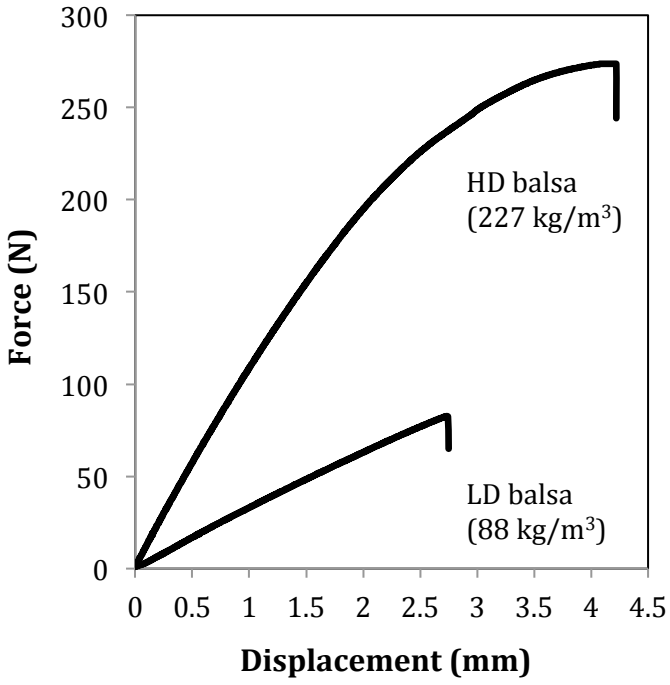
300
250
200
150
100
50
0
Force (N)
0
0.5
1
1.5
2
2.5
3
3.5
4
4.5
Displacement (mm)
HD balsa
(227 kg/m3)
LD balsa
(88 kg/m3)

Fig. 10.

a)

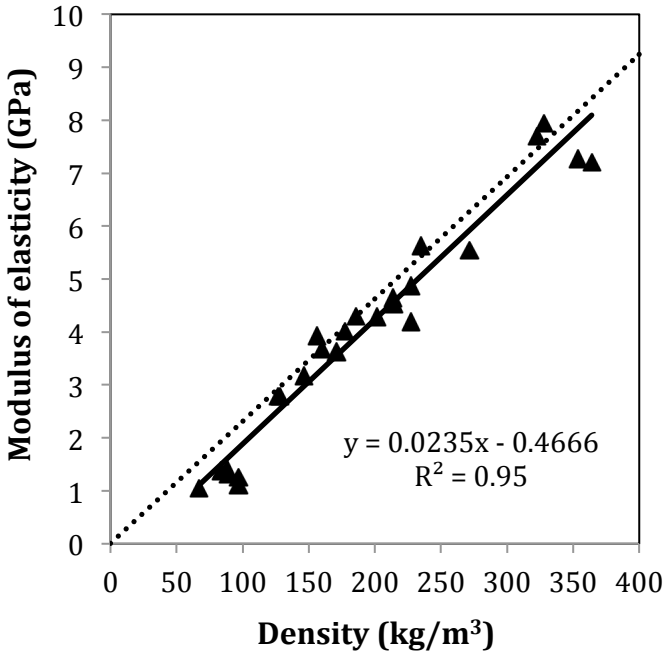
Modulus of elasticity (GPa)
Density (kg/m³)
y = 0.0235x - 0.4666
R² = 0.95
0
1
2
3
4
5
6
7
8
9
10
0
50
100
150
200
250
300
350
400

b)

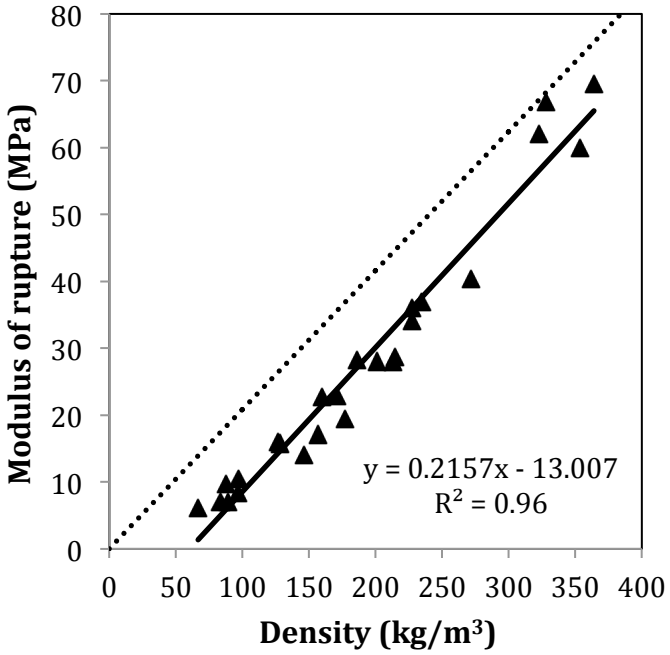
Modulus of rupture (MPa)
Density (kg/m³)
y = 0.2157x - 13.007
R² = 0.96
0
10
20
30
40
50
60
70
80
0
50
100
150
200
250
300
350
400

Fig. 11.

a)

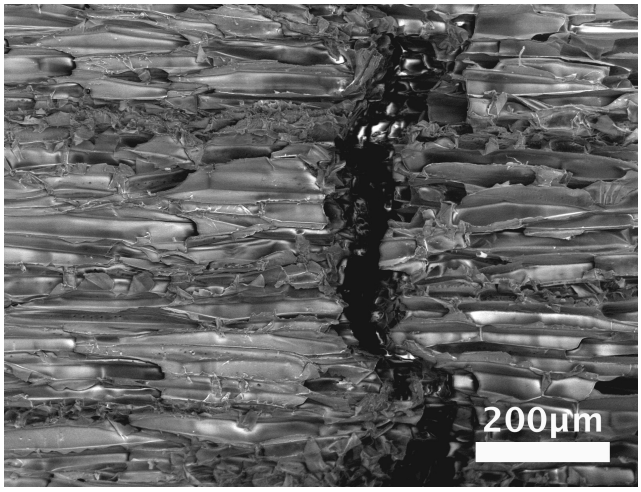

b)

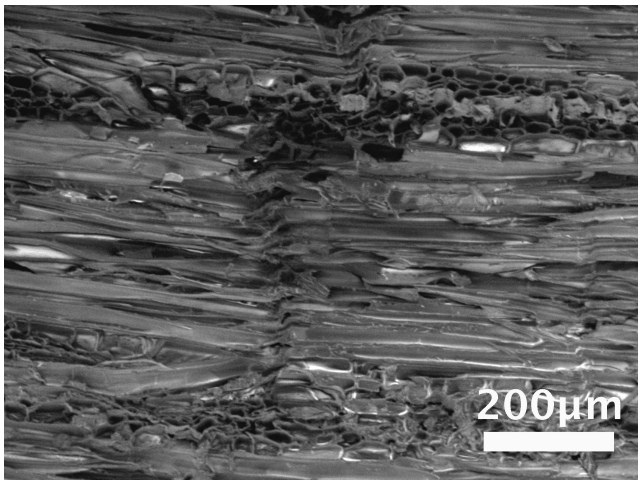

Fig. 12.

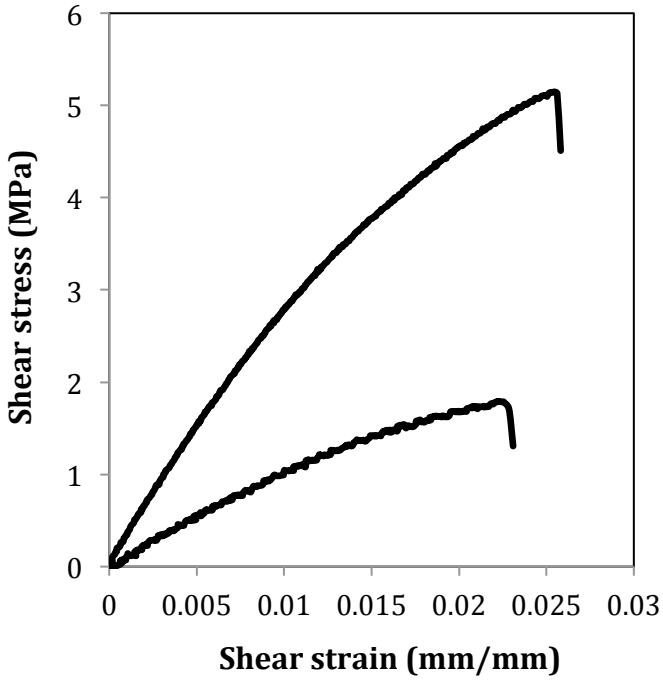
Shear stress (MPa)
6
5
4
3
2
1
0
0
0.005
0.01
0.015
0.02
0.025
0.03
Shear strain (mm/mm)

Fig. 13.

a)

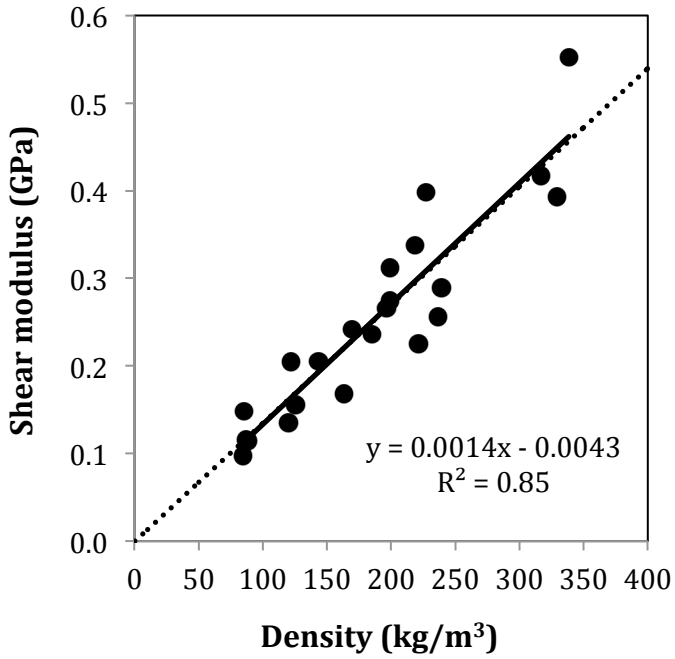
Shear modulus (GPa)
0.6
0.5
0.4
0.3
0.2
0.1
0.0
0
50
100
150
200
250
300
350
400
Density (kg/m³)
y = 0.0014x - 0.0043
R² = 0.85

b)

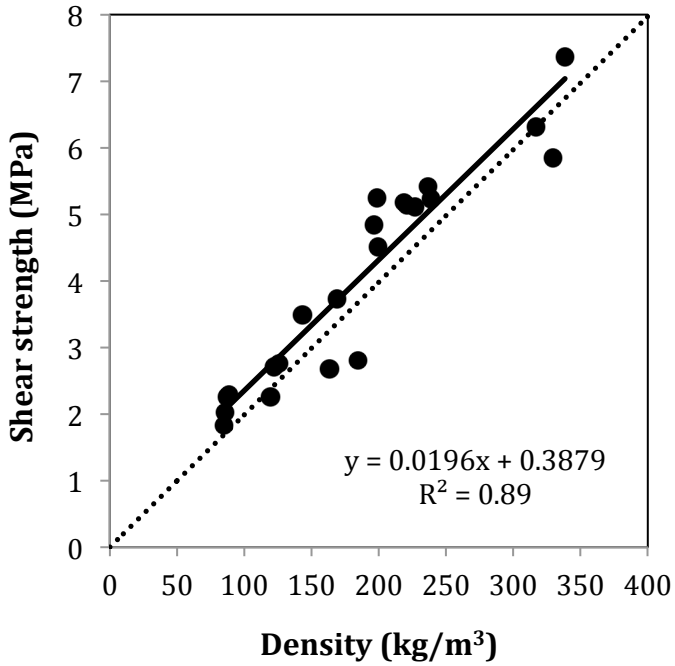
Shear strength (MPa)
8
7
6
5
4
3
2
1
0
0
50
100
150
200
250
300
350
400
Density (kg/m³)
y = 0.0196x + 0.3879
R² = 0.89

Fig. 14.

a)

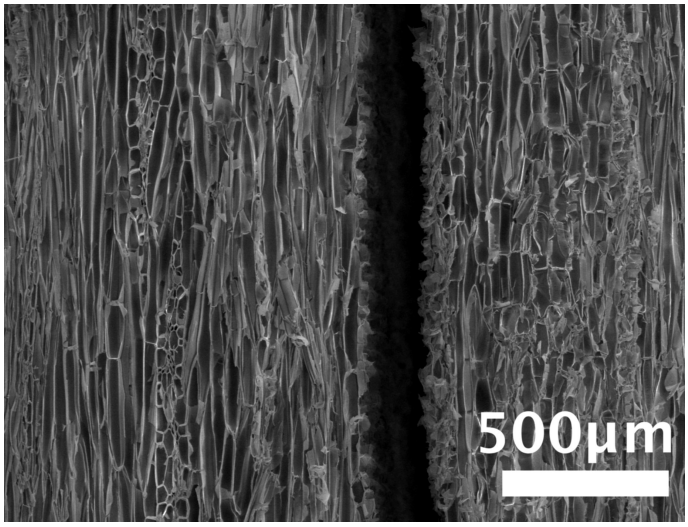

b)

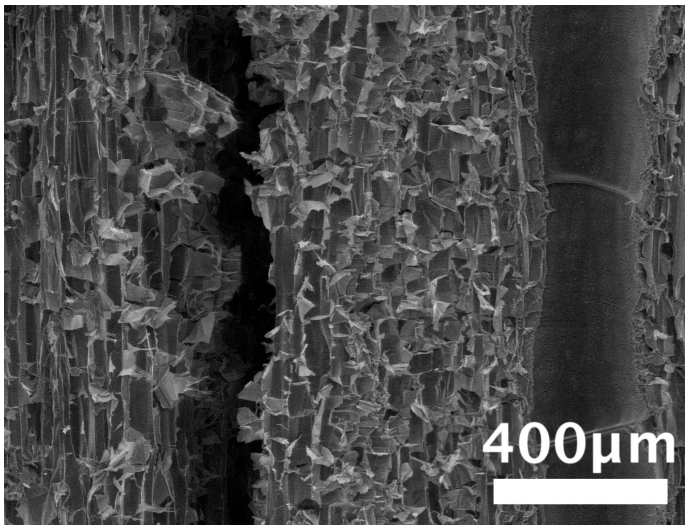

Fig. 14.

c)

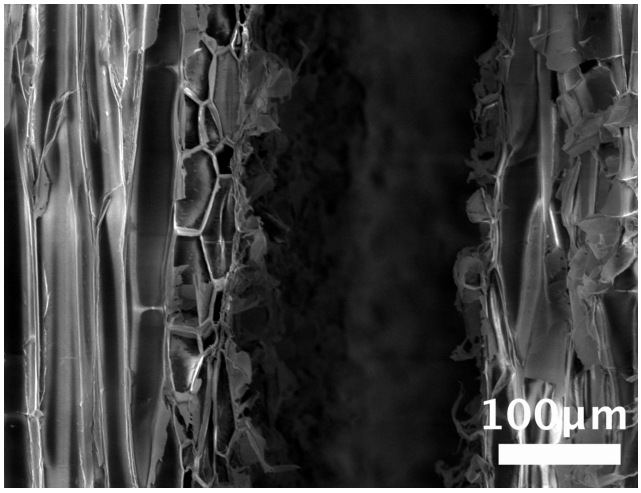

d)

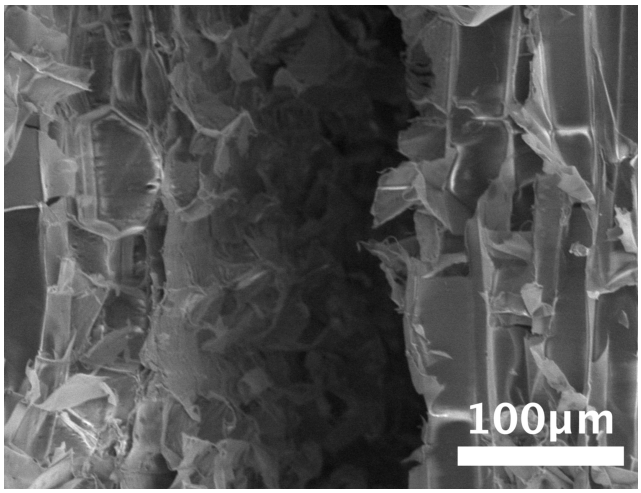

Fig. 15.

a)

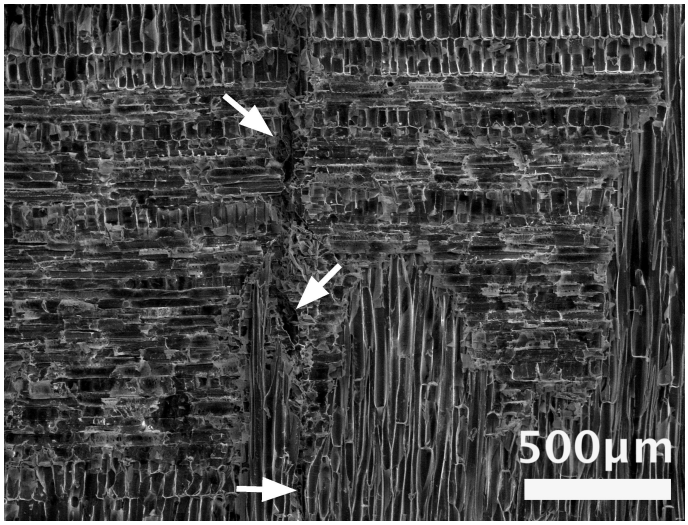

b)

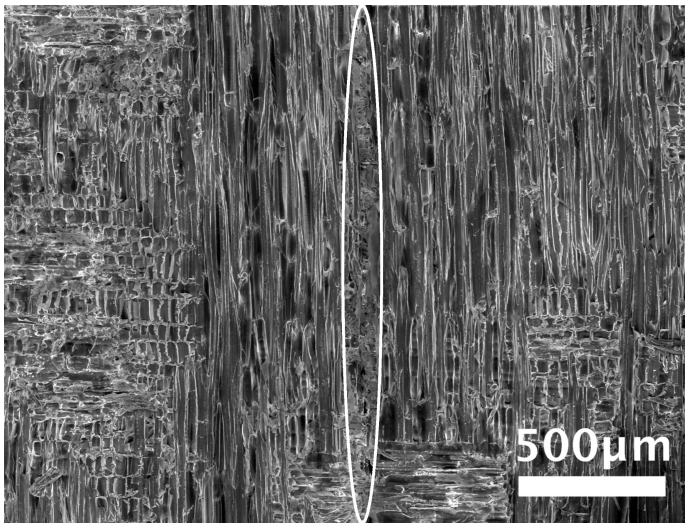

Fig. 15.

c)

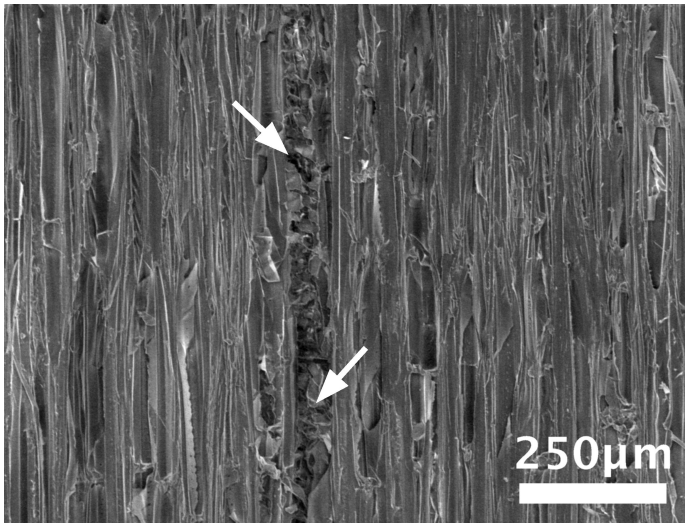

d)